

# Petal-shaped Copper(I) bromide Modified Copper/Graphite as Current Collector for Lithium ion Batteries

He Zhang

Department of Chemical and Environmental Engineering, Hebei Chemical & Pharmaceutical College, Shijiazhuang 050026, China

E-mail: [1197820827@qq.com](mailto:1197820827@qq.com)

Received: 8 November 2021 / Accepted: 25 December 2021 / Published: 2 February 2022

A novel finding, that petal-shaped cuprous bromide (CuBr) particles with a diameter of about 1.5  $\mu\text{m}$  can be prepared onto the commercial copper (Cu) foil surface (denoted as CuBr/Cu) via a soaking method, was reported for the first time in this work. The soaking solution used for producing CuBr only contained 0.5 M  $\text{CuSO}_4$  and a proper amount of HTAB (hexadecyl trimethyl ammonium bromide). And the CuBr coated Cu foils, prepared in the presence of 2 mM, 5mM and 10 mM HTAB were respectively nominated as foil a, b and c. The morphologies and the chemical components of all prepared particles were investigated by using SEM and XRD, respectively, indicating that all prepared particles delivered a petal-shaped morphology and the main chemical substance of all as-prepared particles was CuBr. When being used as the current collectors, all newly prepared foils exhibited an evident promoting effect upon the electrochemical performance of the graphite electrode. For instance, the initial discharge capacity (DC) value of the graphite electrode prepared using foil b (electrode b) at 0.1A  $\text{g}^{-1}$  was measured to be 520 mAh  $\text{g}^{-1}$ , being about 1.49 times higher than that of the graphite electrode assembled using the conventional Cu foil (electrode o) (350 mAh  $\text{g}^{-1}$ ). More importantly, even after 100 cycles, the DC value (141 mAh  $\text{g}^{-1}$ ) of electrode b at 1A  $\text{g}^{-1}$  was about 3.9 time larger than that of electrode o (36 mAh  $\text{g}^{-1}$ ). Presenting a novel method to prepare petal-shaped micron-sized CuBr particles as well as showing a practicable way to improve the electrochemical properties of the graphite electrode were the main dedications of this preliminary work, which was very meaningful to the electrochemical performance improvement of the graphite electrode based lithium ion batteries (LIBs) since no extra energy consumption and no additional preparing processes were required in achieving above works.

**Keywords:** cuprous bromide; surface active agent; immersion process; commercial graphite electrode; lithium ion batteries.

## 1. INTRODUCTION

Although many novel kinds of batteries such as lithium-sulfur battery [1], zinc-air battery [2],

vanadium redox flow battery (VRB) [3], lithium air battery [4], etc., have been developed in recent years, to the best of our knowledge, the main commercialized batteries are still lithium ion batteries (LIBs) and lead-acid batteries (LABs). As far as we know, LIBs, due to its higher energy density and excellent cycling stability, have occupied most parts of the battery market [5]. Of late, using electric vehicles (EV) to replace the fuel vehicle has become a transportation development strategy in many countries so as to greatly reduce the automobile exhaust-derived CO<sub>2</sub> emission. Therefore, as the core component of an EV, LIBs with much higher energy densities have received ever increasing attention, in other words, how to greatly improve the energy density of a LIB has turned into an arduous challenge for all LIBs researchers. As is known to all, besides other parts of a LIB, the anode (negative) part, especially the chemical composition of an anode material, was an important factor which could directly determine the final electrochemical performance of a LIB [6]. To the best of our knowledge, graphite [7], mainly due to its very lower cost and satisfied cycling performance, has been used as an anode material of LIBs ever since the inception of LIBs though many so-called novel kinds of anode materials have been developed in the last several years. Recently, except for utilizing novel kinds of anode materials to substitute for the conventional anode material of graphite, using a modified copper foil to replace the conventional current collector of copper foil was also indicated to be a feasible way to improve the electrochemical performance of a graphite electrode. For example, Yuan's group [8] prepared an array-pattern porous CuO/Cu composite current collector via a chemical etching method in which (NH<sub>4</sub>)<sub>2</sub>S<sub>2</sub>O<sub>8</sub> and micro-bead graphite powders were respectively utilized as the etching reagent and the anode material, and in Yuan's work [8], the initial DC capacity of the graphite electrode constructed by using the resultant current collector was 329.8 mAh g<sup>-1</sup> at 0.2C. Choi and his coworkers [9] successfully fabricated a graphene film modified Cu current collector through a chemical vapor deposition method revealing that both the discharge capacity and cycling stability of the graphite electrode installed by using the as-prepared current collectors were all significantly promoted as compared to the graphite electrode prepared using the pure copper foil. Hu's research group [10] investigated the properties of a rolled electrodeposited (RE) copper foil supported graphite electrode in which the surface morphology modification of the RE copper foil was achieved by using rough surface rollers. And in Hu's work [10], the DC value of the graphite electrode assembled by using RE copper foil was 329.6 mAh g<sup>-1</sup> at 500 mA g<sup>-1</sup>, which was much higher than that of the graphite electrode constituted by using electrodeposited (294.7 mAh g<sup>-1</sup>) copper foil. While, to the best of our knowledge, the approach, of immobilizing petal shaped micron-sized CuBr particles on the surface of the conventional copper foil to remarkably enhance the electrochemical performance of a graphite electrode, has rarely been reported so far.

Cuprous bromide (CuBr) is an important substance which has been widely applied in many research fields. Being employed as a catalyst to catalyze an organic synthesis reaction was reported to be the main application of CuBr in the research field of organic chemistry. For example, a CuBr-catalyzed domino reaction of 2-substituted-3-(1-alkynyl) chromones for preparing functionalized 3-acylfurans was developed by Hu's research group in 2013 [11]. Very recently, the reaction of azidealkyne cycloaddition was also achieved in the presence of CuBr [12]. Also, CuBr can be employed as both optical material [13, 14] and magnetic material [15]. Consequently, many novel strategies were urgently developed with an intention to facily prepare CuBr. Among all developed

CuBr preparation methods, the chemical reaction method, primarily due to its very simple preparation process, was considered as the most preferred method. For instance, as early as 2004, CuBr nanoparticles [16] were prepared through a conventional chemical reaction in which CuO, KBr,  $\text{NH}_2\text{OH}$  and deionized gelatin were utilized as the starting materials. Of late, Prakash' group [17] synthesized nanocrystalline CuBr via a hydrothermal method in which  $\text{CuSO}_4 \cdot 5\text{H}_2\text{O}$ , KBr and glucose were the starting reactants. As far as we know, the preparation of micron-sized CuBr particles via a room temperature soaking method has not yet been reported so far.

Generally, besides the chemical composition, the morphology and the particle size are also the key factors which can significantly affect the final physicochemical properties of the substances studied. Thus, CuBr particles with various morphologies have been prepared in the past two decades. As mentioned earlier, in 2004, CuBr nanoparticles [16] with a cubic morphology were successfully prepared via a traditional chemical reaction. Most recently, Guo's research team [18] prepared tetrahedron-shaped CuBr particles via a chemical reaction in which one soluble divalent copper salt, one organic reducing agent and potassium bromide were employed as the starting materials. To our knowledge, the petal-shaped morphology of micron-sized CuBr particles has not been reported till present.

In this work, a soaking solution containing 0.5 M  $\text{CuSO}_4$  and 2 mM HTAB was made first. And meanwhile, a commercial copper foil was successively rinsed with double distilled water and ethanol generating a well washed Cu foil (denoted as foil o). And then, the air dried foil o was directly placed in the as-prepared soaking solution for 10 min at room temperature to finish the soaking process. After that, the copper foil was took out and washed with double distilled water for two times, and dried in air to produce the final copper foil. When being employed as the graphite electrode current collector, all as-prepared foils exhibited an evident promoting effect on the electrochemical performance of the commercial graphite electrode. Showing a novel method for preparing CuBr at room temperature and developing a new approach to enhance the battery performance of the commercial graphite electrode are the major contributions of this preliminary work.

## 2. EXPERIMENTAL DETAILS

### 2.1 Reagents and materials

The chemical reagents such as  $\text{CuSO}_4$  and hexadecyl trimethyl ammonium bromide (HTAB) were all obtained from Tianjin Reagent Company. Both copper foil and graphite powder were donated by Hebei LingDian New Energy Technology Co., Ltd (Hebei Tangshan, China). Other materials used for assembling the lithium foil based half-cell, such as the metallic Li foil, the separator, acetylene black, PVDF (polyvinylidene fluoride) and the organic electrolyte solution (1 M  $\text{LiPF}_6$ ), were all purchased from Tianjin Lianghuo S&T Developing Co. Ltd (China). All aqueous solutions used in the present work were prepared using secondary distilled water.

## 2.2 Preparation of micron-sized particles coated copper foils

First, a solution containing 0.5 M CuSO<sub>4</sub> and 2 mM HTAB, denoted as solution A, was carefully prepared using CuSO<sub>4</sub> and HTAB. Next, an air dried Cu foil (also denoted as foil o) was directly soaked in solution A for 10 min to complete the soaking process. After being removed from solution A, the Cu foil was carefully rinsed with double distilled water for two times to prepare the final Cu foil. Similarly, solution B and C referred to, respectively, the solution of 0.5 M CuSO<sub>4</sub>+5 mM HTAB and the solution of 0.5 M CuSO<sub>4</sub>+10 mM HTAB. Thus, CuBr coated Cu foils prepared from 0.5 M CuSO<sub>4</sub>+2 mM HTAB, 0.5 M CuSO<sub>4</sub>+5 mM HTAB and 0.5 M CuSO<sub>4</sub>+10 mM HTAB, were nominated as CuBr/Cu-2, CuBr/Cu-5 and CuBr/Cu-10, respectively. For the sake of simplicity, CuBr/Cu-2, CuBr/Cu-5 and CuBr/Cu-10 were respectively labeled as foil a, b and c. For comparison, the well cleaned and dried commercial Cu foil, which was not subjected to the soaking process, was named as foil o.

## 2.3 Characterization

The crystal phase and the chemical compositions of the surface materials of all as-prepared foils were carefully studied by using X-ray diffraction (XRD) (Bruker AXS, D8 ADVANCE, Germany). Scanning electron microscopy (HITACHI, SEM S-570) and transmission electron microscopy (TEM, HITACHI, H-7650) were used to investigate the surface morphologies of all as-prepared foils as well as the size of the prepared particles. The kinds of elements as well as the element contents of the materials peeled off from the surface of the newly prepared foils were studied by using energy dispersive spectrometer (EDS, INCA Energy 350, England). X-ray photoelectron spectroscopy (XPS, Kratos Analytical spectrometer, Al K $\alpha$  radiation) was also used to identify the chemical valences of all elements existing in the scraped substances, so as to further affirm the chemical compositions of the substances scraped from the surface of the resultant foils.

## 2.4 Preparation of as-synthesized foils supported graphite electrode

The commercial graphite electrode was generally constructed by two parts, namely, the anode material of graphite powder and the current collector of the commercial copper foil. Although many new types of anode materials have been created in recent years, to the best of our knowledge, graphite rather than other novel substances was still the main anode material of the commercial LIBs. Thus, the commercial graphite powder was employed as the anode material to prepare the as-prepared foils supported graphite electrodes so as to study the influence of the newly prepared current collectors on the electrochemical performance of the commercial graphite electrode. The preparation procedure of a graphite electrode has been well introduced in the previous work [19]. Generally speaking, a mixture containing the commercial graphite (CG), PVDF and acetylene black (AB) was prepared first in which the mass ratio of CG:PVDF:AB was 8:1:1. And then, a very small amount of N-methylpyrrolidone (NMP) was added carefully into above resulting mixture under stirring to produce a mud like paste. Subsequently, the resulting paste was immediately painted on the surface of an as-prepared foil with

the help of a glass sheet. Next, the as-assembled electrode was dried in a vacuum oven at 120 °C for 6 h generating a well dried graphite electrode. Approximately, the loading amount of the commercial graphite powder per square centimeter of each current collector was estimated to be 1.5 mg. The graphite electrodes assembled by using foil o, a, b and c were, respectively, labeled as electrode o, a, b and c.

The half-cell consisting of one above as-prepared electrode and a metallic lithium foil was assembled in a N<sub>2</sub> filled glove box (ZKX, Nanjing NanDa Instrument Plant, China). That is to say, under the protection of nitrogen gas, the metallic lithium foil, organic electrolyte, separator, organic electrolyte and one as-prepared electrode were sequentially and tightly packed together producing a half-cell. The organic electrolyte and separator used in the assembled half-cell were respectively 1 M LiPF<sub>6</sub> and Celgard 2400. The organic solvent used for dissolving LiPF<sub>6</sub> was a mixed solvent which mainly contained ethyl methyl carbonate (EMC), ethylene carbonate (EC), vinylene carbonate (VC) and dimethyl carbonate (DMC). Apparently, the metallic lithium foil acted as both a negative electrode and a reference electrode. Therefore, all potential values reported in this work were relative to that of the metallic lithium foil. A charge/discharge equipment (CT-3008W-5V20mA-S4, Shenzhen Neware Electronics Co., Ltd. China) was used to conduct the galvanostatic charge-discharge experiments in which the potential window was from 0.01 V to 3 V. The current densities used in the galvanostatic charge-discharge tests were 0.1, 0.3, 0.5, 1 and 2 A g<sup>-1</sup>, respectively.

Cyclic voltammetry (CV) and electrochemical impedance spectroscopy (EIS) were all carried out on an electrochemical workstation (denoted as EW) (CHI 660E, Shanghai Chenhua Apparatus, China). In this experiment, the green clip of the EW was connected to the working electrode, and both the red clip and white clip of the EW were connected together to the negative electrode (i.e., the metallic lithium foil). In the EIS measurement, the frequency range and the amplitude of alternating current (AC) were, respectively, 0.1~10<sup>5</sup> Hz and 5 mV.

### 3. RESULTS AND DISCUSSION

#### 3.1 SEM characterization

The photos of all samples involved in the preparation process are successively collected in Figure 1a. Apparently, the solution containing 0.5 M CuSO<sub>4</sub> and HTAB was a dark blue solution. For all prepared foils, no evident color differences were found before and after the soaking process. To one's surprise, after being dried at 120° in a vacuum oven for 6 h, the color of the prepared foils, as shown by rightmost photos, varied markedly. In the absence of HTAB, no color change was found for foil o even after the vacuum drying treatment. Interestingly, for other three prepared foils, the color of the as-prepared foils gradually deepened with increasing the concentration of HTAB, that is, a dark coppery color for foil a, a light brown color for foil b and a dark brown color for foil c, showing a tendency varying from the coppery color to a dark brown color.

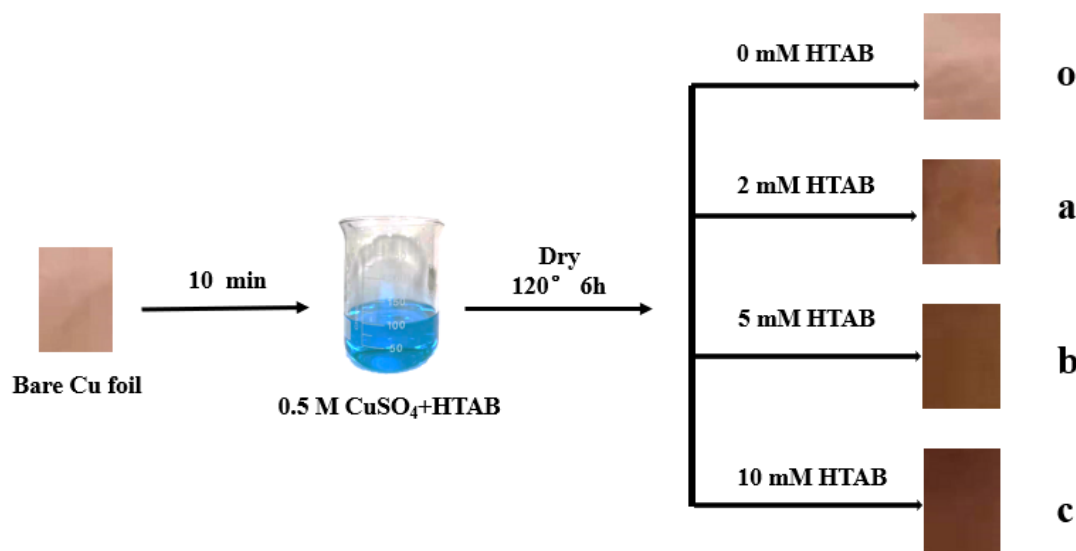


**Figure 1a.** Photos for the bare copper foil, the soaking solution as well as all studied Cu foils. As a note, prior to taking pictures, all resultant foils were dried at  $120^{\circ}$  in a vacuum oven for 6 h. Photo o, a, b and c corresponded to foil o, a, b and c.

The surface SEM images of all studied copper foils are presented in figure a of Fig.1b. Some irregular streaks were observed in the SEM images of foil o suggesting that no evident particles existed on the conventional copper foil surface (image o and o'). As shown by image a and a', some huge flaky particles and some irregular blocky-shaped particles appeared on foil a surface demonstrating that some new substances were synthesized on the surface of the conventional copper foil after the simple soaking process. As presented by image b and b', a great deal of petal-shaped particles were fabricated on the surface of foil b generating an uneven surface. And the average diameter of those petal-shaped particles was close to  $1.5 \mu\text{m}$  suggesting that all prepared particles were micron-sized particles. In the case of foil c (image c and c'), those petal-shaped particles were closely connected together forming a novel superficial coat. Thus, it was reasonable to conclude that the concentration of HTAB was a key parameter which not only influenced the surface morphologies of the prepared foils but also remarkably affected the particle size of the as-synthesized particles. As a representative, TEM images of the petal-shaped micron-sized particles of foil b are presented in figure b of Fig.1b. In the TEM image with a scale of  $2 \mu\text{m}$ , a large number of small particles were clearly exhibited suggesting that all those petal-shaped micron-sized particles were constructed by numerous nanoparticles. More interestingly, besides some evident rod-like particles, many lasso-shaped nanoparticles appeared in the TEM image with a scale of  $500 \text{ nm}$ . The average diameter and the internal diameter of the lasso-shaped nanoparticles were estimated to be  $42 \text{ nm}$  and  $28 \text{ nm}$ , respectively, again indicating that the prepared lassoes were nano-lasso, which probably could be applied as the capture agents in the nano drug field.

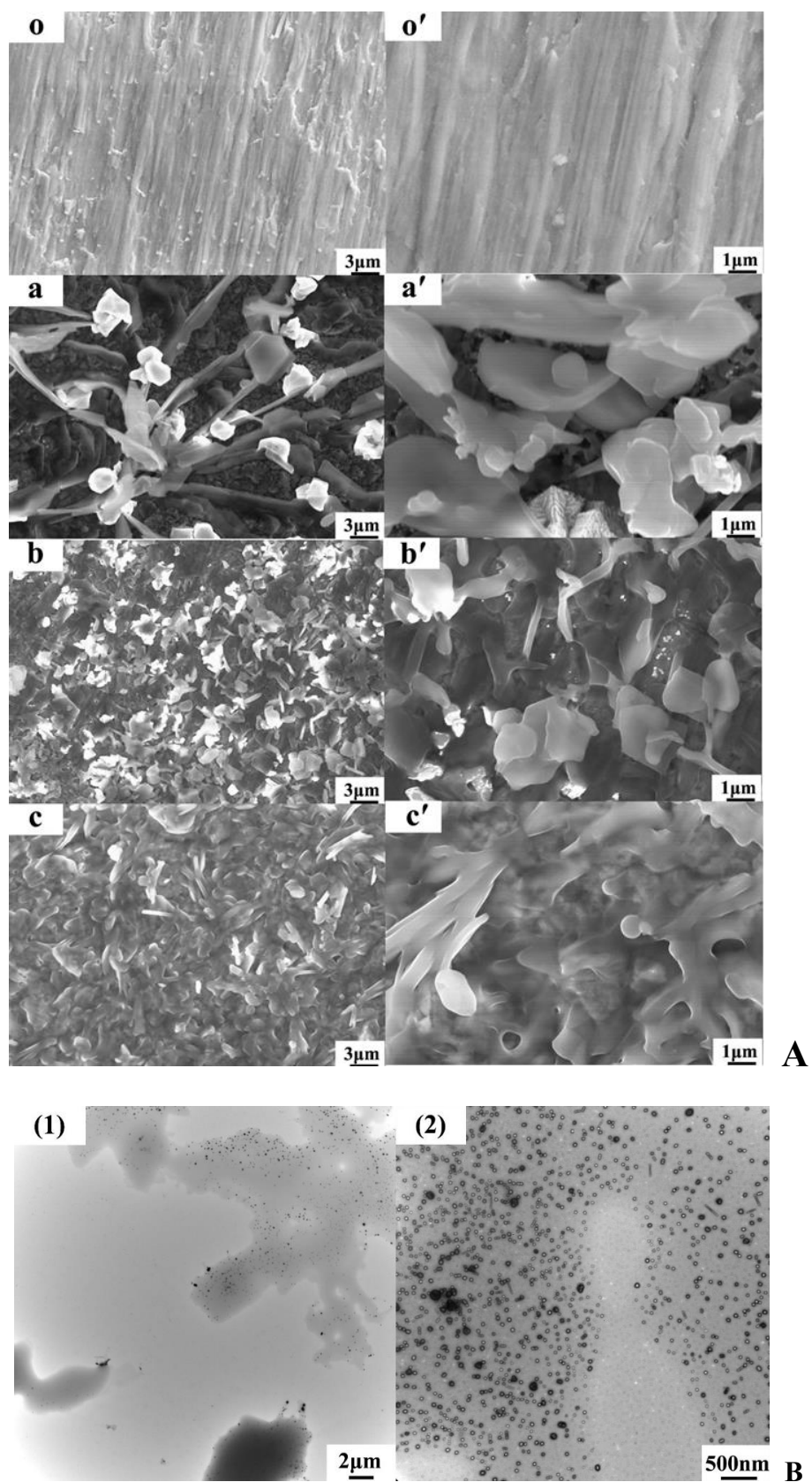


**Figure 1b.** (a) SEM images with a scale of 3 μm and that of 1 μm for all the studied foils. Image o and o', a and a', b and b', c and c' corresponded to foil o, a, b and c. (b) TEM images with a scale of 2 μm (image 1) and that of 500 nm (image 2) for the substances peeled off from the surface of foil b.

### 3.2 Characterization of all as-prepared samples

XRD patterns for the substances peeled off from all prepared foils as well as the standard XRD pattern for CuBr are given in Fig.2a.

For all patterns, a broad diffraction peak located at  $2\theta$  value ranging from  $20^\circ$  to  $30^\circ$  was displayed clearly which was generally attributed to the existence of amorphous carbon or graphitized carbon [20]. For foil b (pattern b), three diffraction peaks located at  $43.4^\circ$ ,  $50.6^\circ$  and  $74.3^\circ$  were well, respectively, assigned to the (111), (200) and (220) facet of the metallic Cu (JCPDS, No.1-1241), indicating that most materials of the scraped substances from foil b were the metallic Cu. While for foil c (pattern c), only one diffraction peak positioned at  $43.4^\circ$  was displayed, and no evident typical diffraction peaks assigned to metallic Cu or CuBr were observed implying that less amount of substances with higher crystallinity were formed on the commercial copper foil surface. The difference in the XRD patterns indicated that the chemical ingredients of the substances formed on the surface of the prepared foils were different from each other.

EDS patterns of the substances peeled off from the prepared foils are given in Fig.2b. For foil o, only the peaks belonging to Cu were displayed suggesting that the commercial copper foil was uniquely constituted by the metallic Cu. For other three prepared foils, besides the peaks assigned to Cu element, two main peaks indexed as the element of Br and C were respectively clearly exhibited substantially implying that some substances were really immobilized on the surface of the commercial copper foil. The existence of C element was mostly attributable to the residual of HTAB on the surface of copper foil, being in line with the fact that the diffraction peaks assigned to C were displayed in the XRD patterns of all resultant foils.

The atomic contents of Cu, Br and C in the scraped substances were measured to be 39%, 12%, 41% for foil a, and 26%, 9%, 61% for foil b, and 12%, 9%, 77% for foil c, and 86%, 0, 9% for foil o, respectively.

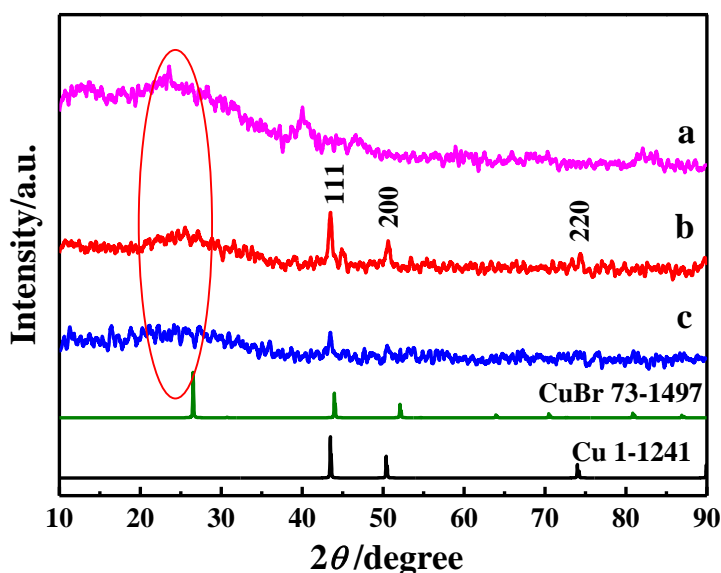


**Figure 2a.** XRD patterns of the substances peeled off from the surface of the as-prepared foils. Pattern a, b and c corresponded to the surface substances obtained from foil a, b and c.

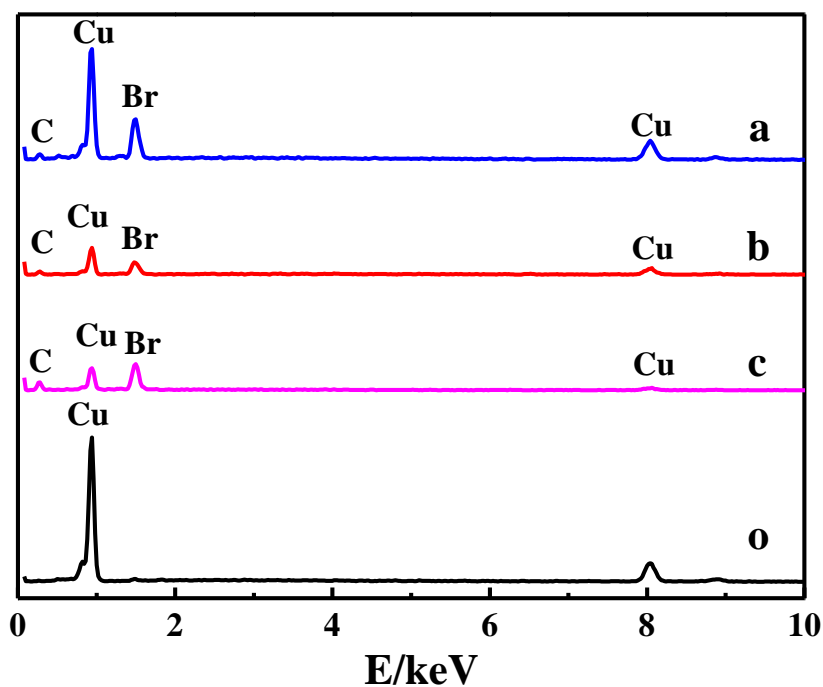
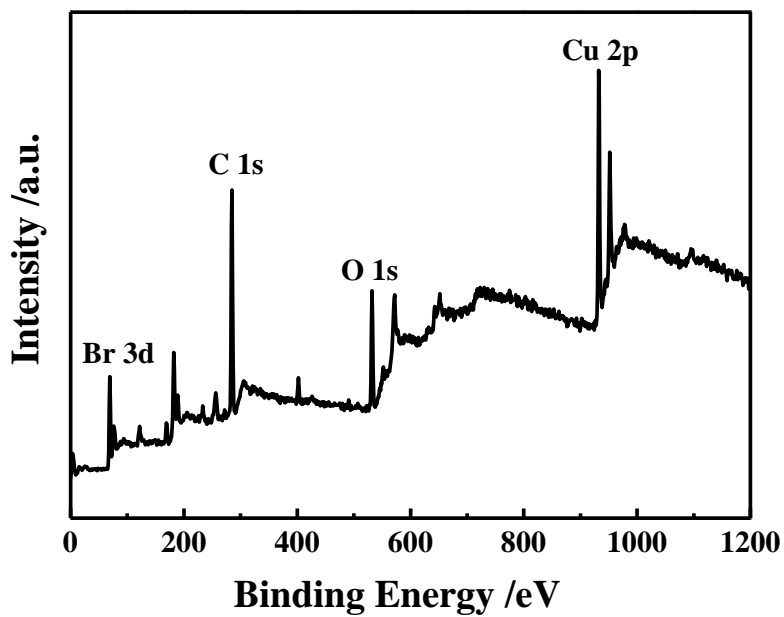


**Figure 2b.** EDS patterns of the substances scraped from the surface of the as-prepared foils. Pattern o, a, b and c corresponded to the surface substances scraped from foil o, a, b and c.

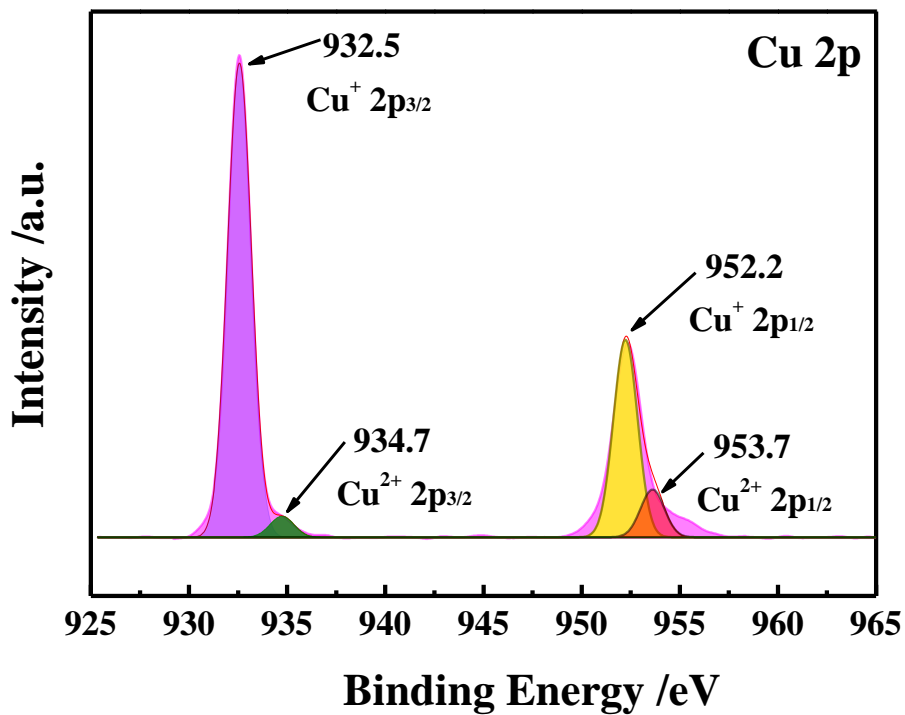
The atomic contents of O element in the scraped substances for foil a, b, c and o were, respectively, recorded to be 4.6%, 2.2%, 0.6% and 2.8%. Thus, it was concluded, based on the atomic content of O element in foil o, that the presence of very small amount of O element should be stemmed from the adsorbed CO<sub>2</sub> or tiny amount of copper oxides. Therefore, the main components of the scraped substances should be metallic Cu, carbon material and CuBr (or CuBr<sub>2</sub>).

XPS patterns of the surface substances of foil b, as a representative, are plotted in the figures of Fig.3 so as to identify the chemical valences of the elements, further confirming the chemical compositions of the substances anchored on the surface of foil b after the soaking treatment. The presence of Cu, Br, C and O elements in the surface substance of foil b was effectively indicated by the exhibition of their characteristic peaks in the wide scan XPS spectra of figure a, which was well consistent with the EDS results (Fig.2b). The high resolution XPS spectra for Cu 2p core is presented in figure b in which two huge peaks positioned at 932.5 eV (Cu 2p<sub>3/2</sub>) and 952.2 eV (Cu 2p<sub>1/2</sub>) were exhibited explicitly indicating that the main chemical valence of Cu element was +1[21]. Meanwhile, other two small binding energy (BE) peaks were respectively displayed at 934.7 eV (Cu 2p<sub>3/2</sub>) and 953.7 eV (Cu 2p<sub>1/2</sub>) indicating the existence of very small amount of Cu<sup>2+</sup> [21].

(a)



(b)



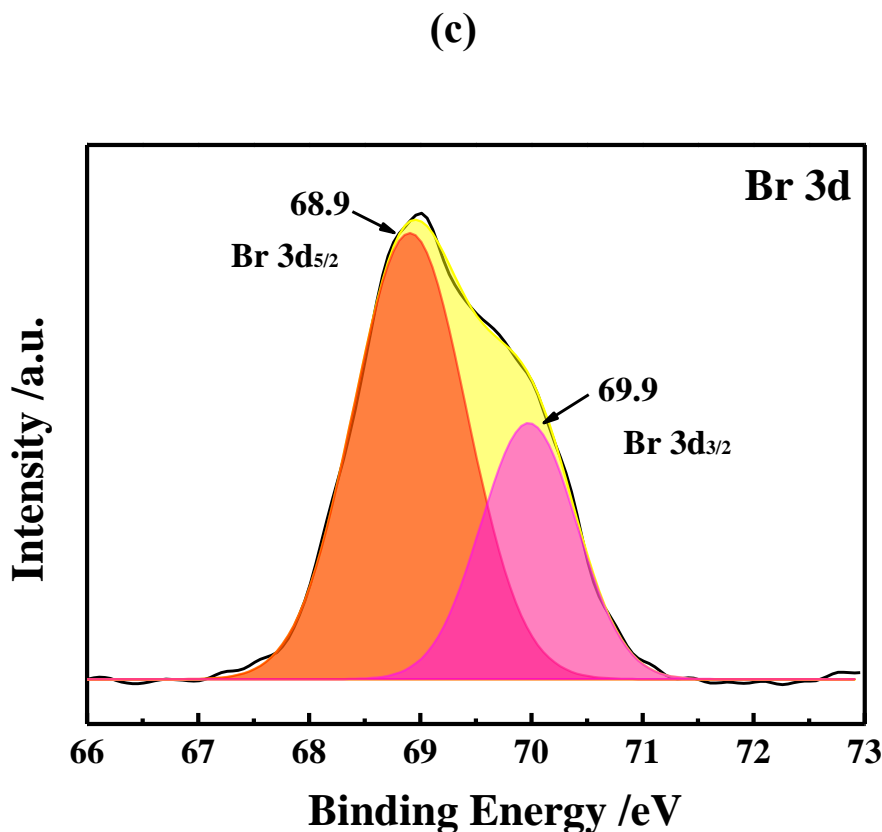


**Figure 3.** XPS survey spectra for the substances scraped from the surface of foil b. (a) Wide scan XPS survey spectra; (b) High resolution Cu 2p spectrum of XPS spectra (c) High resolution Br 3d spectrum of XPS spectra.

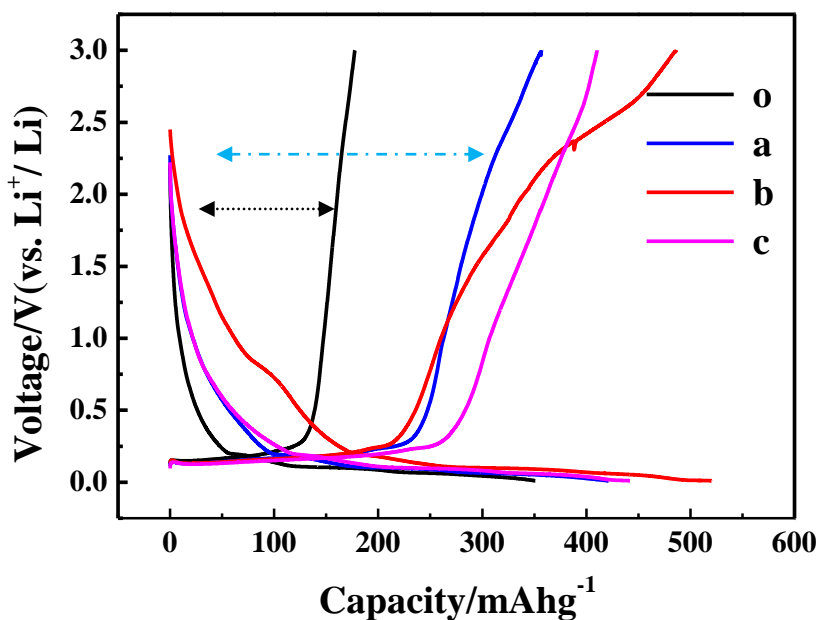
The characteristic satellite peak (943.67 eV) assigned to  $\text{Cu}^{2+}$  was not observed [21, 22] implying that the content of  $\text{Cu}^{2+}$  was very lower relative to that of  $\text{Cu}^+$ . As shown by the XPS spectra of Br element (figure c of Fig.3), the BE peaks located at about 68.9 and 69.9 eV were, respectively, originated from Br  $3d_{5/2}$  and Br  $3d_{3/2}$ , indicating the presence of  $\text{Br}^-$  in the scraped substances of foil b [23]. Therefore, being combined with the EDS result (Fig.2b), it could be concluded that most substances appearing on the surface of foil b were CuBr. That is, those petal-shaped micron-sized particles appearing on the surface of foil b were CuBr particles. As far as we know, the preparation of petal-shaped micron-sized CuBr particles via a room temperature soaking method has never been reported previously. In other words, the chemical reaction, namely,  $\text{Cu}^{2+} + \text{Br}^- + \text{Cu (s)} \rightarrow \text{CuBr} \downarrow$ , was achieved at room temperature via a simple soaking process in the present work, which was a novel finding.

### 3.3 Electrochemical performances of the graphite electrode assembled using the novel foils

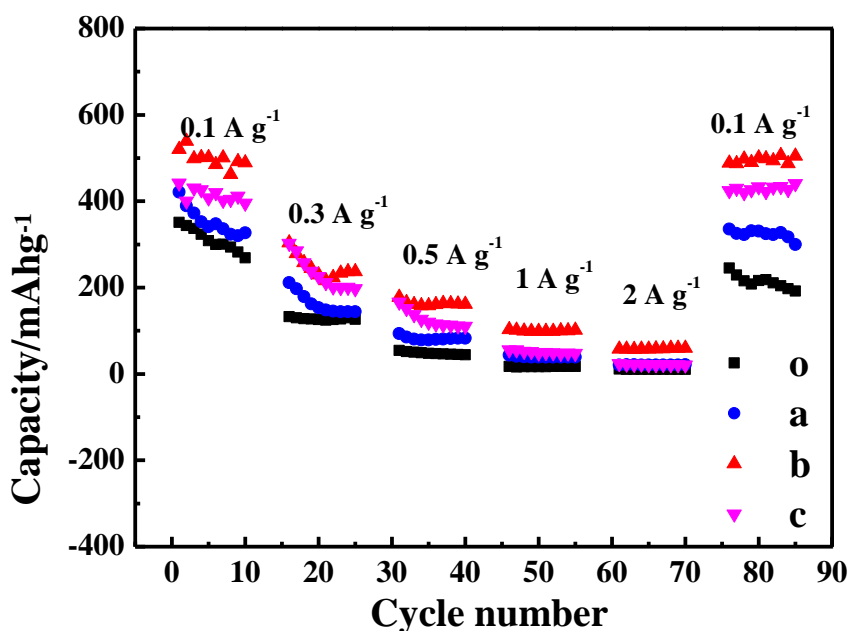
Figure a of Fig.4 shows the initial charge-discharge profiles of the graphite electrodes prepared using various foils which were measured in the potential window of 0.01-3V under the current density of  $0.1 \text{ A g}^{-1}$ .

For all profiles, the potential plateaus appearing in the discharging and charging process were respectively positioned at about 0.1V and 0.17 V. The shape of the initial charge-discharge curves shown in figure a was very similar to that of the microsphere graphite [24, 25], which strongly indicated that graphite was the main lithium ion storage material rather than the newly prepared micron-sized CuBr particles. The initial DC values of the studied graphite electrodes at 0.1A g<sup>-1</sup> were measured to be 350.7, 421.2, 520.2 and 441.8 mAh g<sup>-1</sup> for electrode o, a, b and c, respectively.

(a)



(b)



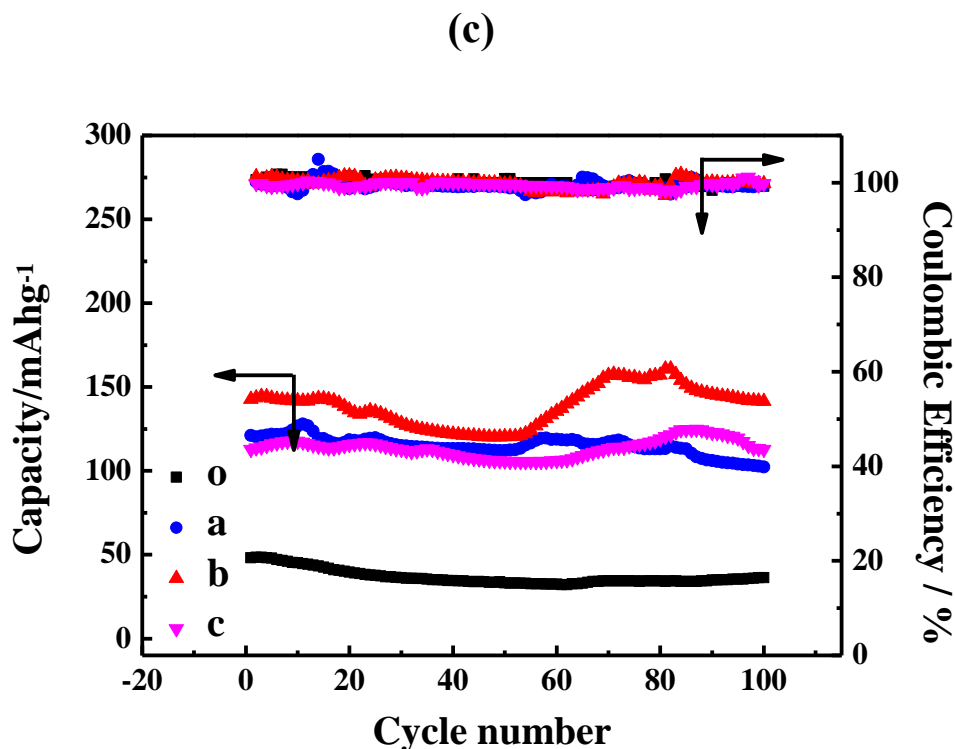


**Figure 4.** Results of electrochemical measurements. **(a)** The initial charge-discharge profiles for all studied graphite electrodes which were measured at  $0.1 \text{ A g}^{-1}$  within the potential range of 0.01-3.0 V. Curve o, a, b and c corresponded to electrode o, a, b and c. **(b)** Rate capabilities of all studied graphite electrodes. In this measurement, the current densities of 0.1, 0.3, 0.5, 1 and  $2 \text{ A g}^{-1}$  were respectively applied. In each rate test, the assembled half-cells were cycled for 10 cycles. After all above experiments, the applied current density was reverted to be  $0.1 \text{ A g}^{-1}$  and the corresponding results are displayed at the right side of this figure. **(c)** Cycling performances of all studied graphite electrodes which were measured at  $1 \text{ A g}^{-1}$  for 100 cycles. The upper curves in figure c described the relationship between the cycling number and coulombic efficiency. Plot o, a, b and c corresponded to the case of using electrode o, a, b and c.

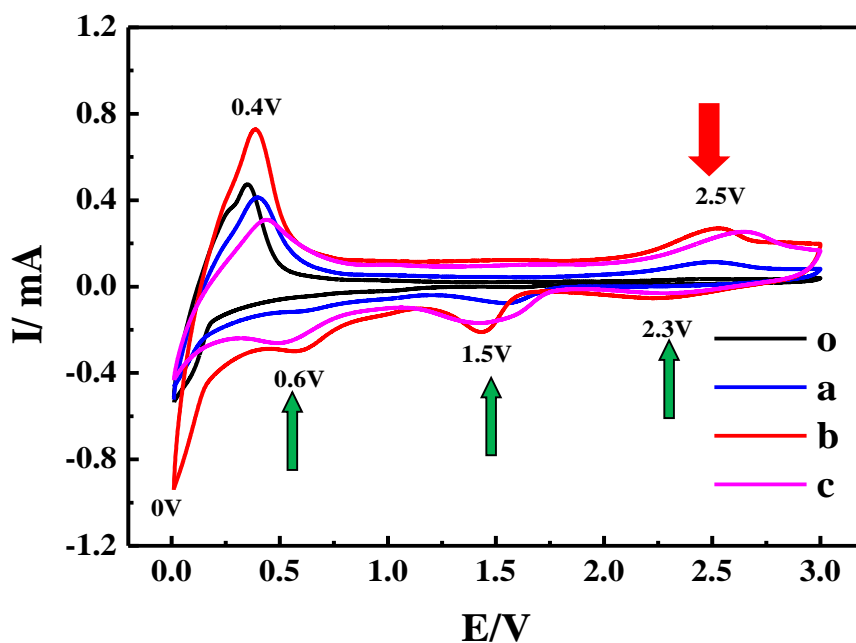
That is, the DC values of all the graphite electrodes prepared using the newly prepared foils were significantly higher than that of the conventional graphite electrode, which strongly indicated that some novel substances as anode materials have been activated to take part in the delithiation/lithiation process of electrode a, b and c. Generally, the potential plateau appearing in the charge-discharge profiles corresponded to a two-phase transformation reaction between a Li containing substance and its corresponding Li free substance [26]. Evidently, as shown by the two double arrow lines in figure a, the length of the potential plateau for the electrode o was rather smaller than that of other three electrodes. This result effectively indicated that as compared to the case of using the conventional copper foil, more amounts of lithium ions were activated to be involved in the charging/discharging process when employing the newly prepared foils as the current collectors of the graphite electrode.

The rate capabilities of the graphite electrodes assembled using the as-prepared foils were also compared with that of the graphite electrode assembled employing the conventional copper foil and the results are shown in figure b of Fig.4. In the rate capability measurements, the current densities used were 0.1, 0.3, 0.5, 1 and  $2 \text{ A g}^{-1}$ , respectively. And in each rate test, the half-cell was cycled for 10

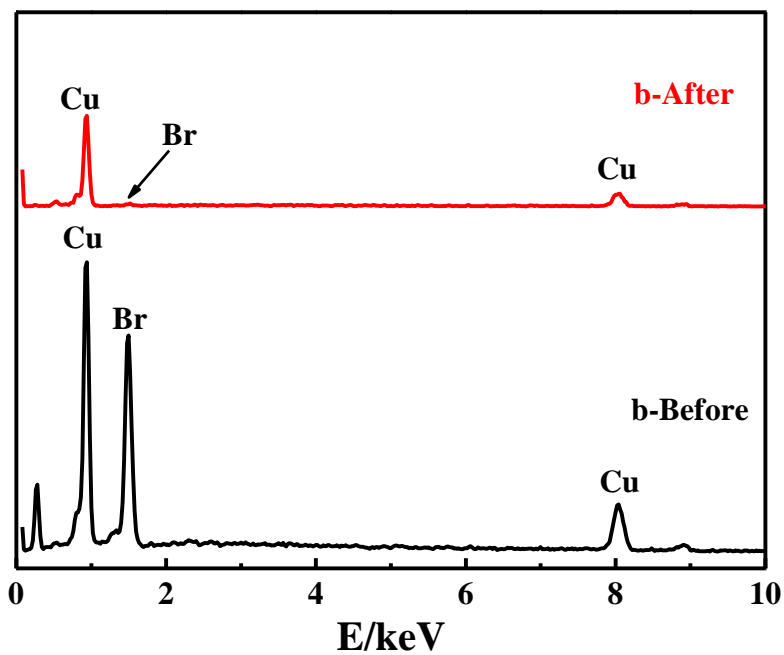
cycles. Apparently, in each test, the DC values of electrode a, b and c were all evidently higher than that of electrode o, substantially indicating that using the as-prepared foils to replace the conventional copper foil was a practicable way to greatly improve the rate capability of the graphite electrode. Obviously, electrode b showed the largest DC value among all studied electrodes. Be noted that, even at the current density of  $2 \text{ A g}^{-1}$ , the DC value delivered by electrode b ( $58 \text{ mAh g}^{-1}$ ) was still about 3 times higher than that of the traditional graphite electrode (electrode o) ( $20 \text{ mAh g}^{-1}$ ). Interestingly, when the current density was backed to be  $0.1 \text{ A g}^{-1}$ , the electrochemical performances of all electrodes were kept almost unchanged. For example, the DC value of electrode b was still maintained to be about  $510 \text{ mAh g}^{-1}$  as the current density was returned to be  $0.1 \text{ A g}^{-1}$ , which was close to the initial DC value of  $520 \text{ mAh g}^{-1}$ . In other words, the utilization of as-prepared novel foils to substitute for the conventional copper foil did not damage the reproducibility of the conventional graphite electrode.

The cycling stabilities of all studied electrodes are compared and the results are given in figure c of Fig.4 in which the current density and the cycling number are respectively  $1 \text{ A g}^{-1}$  and 100. In the whole testing period, electrode b (red curve) delivered the largest DC value among all studied electrodes. For instance, the DC values at  $1 \text{ A g}^{-1}$  of electrode o, a, b and c after 100 cycles varied from 48 to  $36 \text{ mAh g}^{-1}$ , from 121 to  $102 \text{ mAh g}^{-1}$ , from 143 to  $141 \text{ mAh g}^{-1}$ , and from 114 to  $112 \text{ mAh g}^{-1}$ , respectively, approximately corresponding to a retention rate of 75%, 84%, 98% and 99%. In addition, as shown by the upper part of figure c, the Coulomb efficiency (CE) values of all studied electrodes were close to 100 % suggesting that no evident electricity quantity loss occurred in the entire cycling performance.

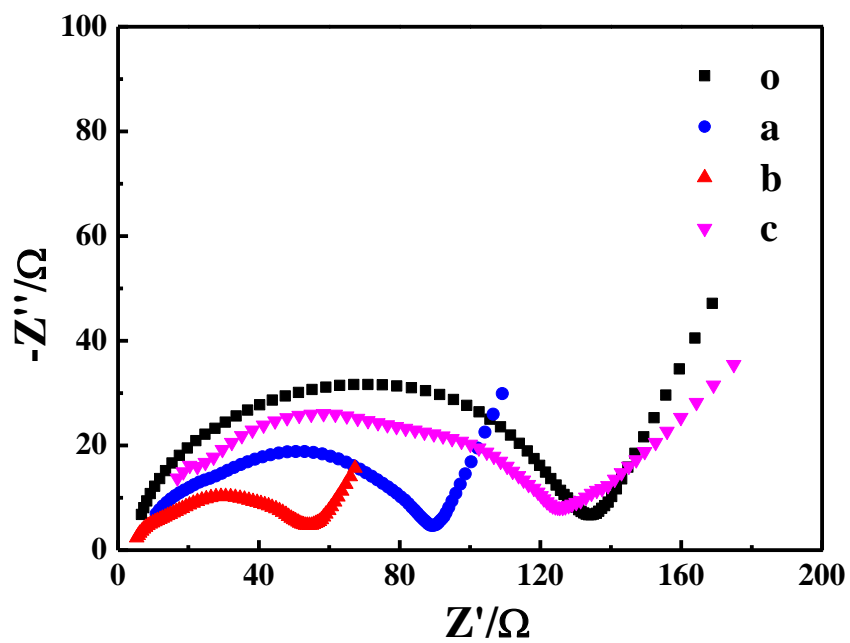
(a)



(b)



(c)



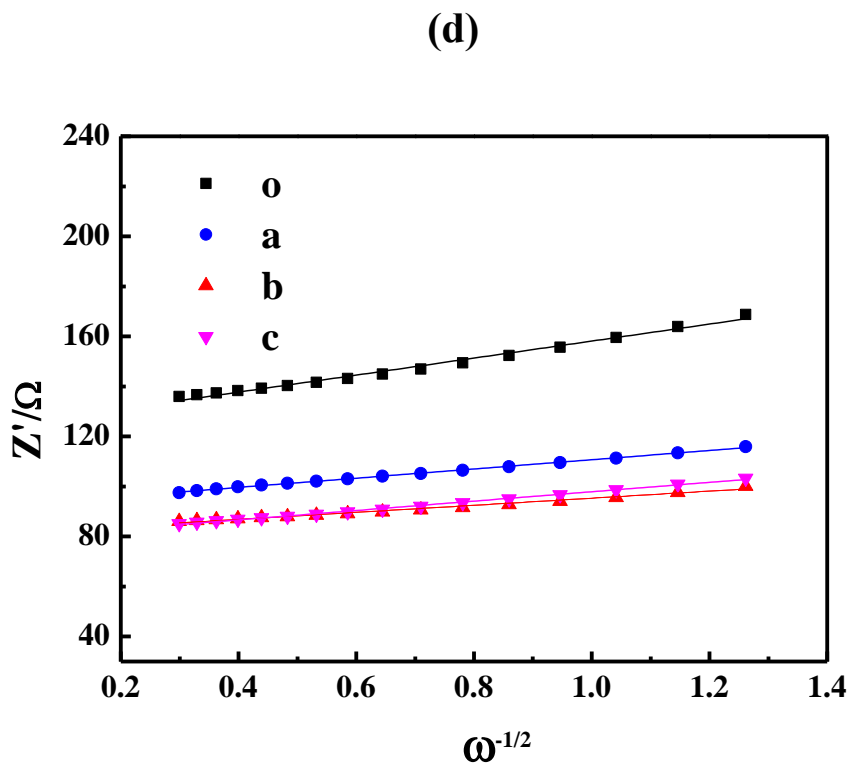


**Figure 5.** (a) Cyclic voltammetry (CV) curves of all studied electrodes which were recorded at the scan rate of  $1 \text{ mV s}^{-1}$  in the potential range from 0.01V to 3.0V. Curve o, a, b and c corresponded to electrode o, a, b and c. (b) EDS patterns of the substances peeled off from the surface of foil b. Pattern b-before corresponded to the substances scraped from the surface of the newly prepared foil b. Pattern b-after corresponded to the substances scraped from the surface of foil b after 100 cycles at  $1 \text{ A g}^{-1}$ . (c) Nyquist plots for all studied graphite electrodes. Plot o, a, b and c corresponded to electrode o, a, b and c. (d) Curves describing the relationship between  $Z'$  and  $\omega^{-1/2}$ . Curve o, a, b and c corresponded to electrode o, a, b and c.

The CV curves of all prepared electrodes are compared in figure a of Fig.5 in which the potential scan rate was  $1 \text{ mV s}^{-1}$ . For electrode o (black curve), the electro-oxidation peak displayed at around 0.40 V in the positive potential scanning was generally attributed to the deintercalation of Li from the graphite [25], and in the negative potential scanning, the huge electro-reduction peak positioned at 0 V was correspondingly stemmed from the formation of  $\text{LiC}_6$  [25], showing a CV curve shape similar to that of the graphite electrode [27].

While for other three electrodes, except for the electro-oxidation peak centered at about 0.40V, a novel small electro-oxidation peak appeared at 2.5 V (as shown by the red arrow), strongly indicating that some novel substances have participated in the deintercalation process of Li ion. Interestingly, in the negative potential scanning, besides the huge electro-reduction peak at about 0.01 V, three electro-reduction peaks were successively observed at about 0.60 V, 1.5V and 2.3 V (as shown by the green arrows), indicating that three kinds of novel substances have been triggered to participate in the discharging process. The differences in the CV curve shape at least indicated that the charge-discharge mechanism of the conventional graphite electrode (electrode o) was different from that of the graphite electrode prepared using the newly synthesized foils. Meanwhile, electrode b exhibited the largest CV

curve area among all studied electrodes implying that the largest amounts of lithium ion were transferred in electrode b. This is, when employing the newly prepared foils as the current collectors of the conventional graphite electrode, some unknown substances were activated to take part in the intercalation/deintercalation process of  $\text{Li}^+$ , which just supported the fact that the discharge capacities delivered by the graphite electrodes assembled using the newly prepared foils were all obviously larger than that of the conventional graphite electrode.

Also, EDS results for the surface substances peeled off from foil b before and after 100 cycles at  $1 \text{ A g}^{-1}$  are given in figure b of Fig.5. Obviously, prior to the long-term cycling test, the huge peaks assigned to both Cu and Br elements are clearly displayed indicating the formation of CuBr (also on the basis of the XPS analysis (figures of Fig.3)) on the surface of the conventional copper foil, while, after the cycling measurement, the peaks indexed as Br element almost vanished. This result strongly suggested that the newly prepared CuBr particles have participated in the charge-discharge process, or, the as-prepared CuBr was totally consumed in the cycling process, which was well in accordance with the fact that several novel CV peaks were exhibited in the CV curve of electrode b (figure a of Fig.5).

Nyquist plots for all studied electrodes are collected in figure c of Fig.5. For all prepared electrodes, the Nyquist plot was constructed by a semicircle and a sloped line, very resembling the shape of the previous Nyquist plot for a half-cell [28, 29]. In general, the diameter of the semicircle was approximately equal to the value of charge transfer resistance ( $R_{ct}$ ), and the sloped line appearing in the lower frequency region was originated from the presence of lithium ion diffusion (also called as Warburg resistance) in the electrode materials [30]. The values of  $R_{ct}$  for electrode o, a, b and c were roughly evaluated to be about 135, 89, 54 and 124  $\Omega$ , respectively. That is, electrode b had the smallest value of  $R_{ct}$  among all studied electrodes implying that the charge-discharge process occurring in electrode b had a faster kinetics as compared to other electrodes. It should be noted that the  $R_{ct}$  value of electrode b (54  $\Omega$ ) was significantly lower than that of previously reported carbon-modified graphite (79.8  $\Omega$ ) electrode [25]. Also, the  $R_{ct}$  values of electrode a, b and c were all evidently smaller than that of electrode o which strongly indicated that utilizing the newly prepared foils as the novel current collectors of the traditional graphite electrode was a practical approach for greatly decreasing the charge transfer resistance of the conventional graphite electrode.

On the basis of the previous work [31], the lithium ion diffusion coefficient ( $D_{\text{Li}^+}$ ) values of all studied electrodes were also calculated using the following equations. Firstly, the value of  $\sigma$  was estimated using equation (1) [31], namely,

$$Z_e = R_s + R_{ct} + \sigma \omega^{-1/2} \quad (1)$$

In above equation, the scientific meanings of  $Z_e$ ,  $R_s$ ,  $R_{ct}$  and  $\omega$  have been well introduced in Ref.31. That is, the value of  $\sigma$  was just equal to the slope of the line describing the relationship between  $Z'$  and  $\omega^{-1/2}$ . Next, the  $\sigma$  value was put in equation (2) [30, 31] to calculate the final value of  $D_{\text{Li}^+}$ .

$$D_{\text{Li}^+} = \frac{(RT)^2}{2An^2F^2C_{\text{Li}^+}\sigma^2} \quad (2)$$

In equation (2), R and T corresponded to the Joule constant and absolute temperature,

respectively.  $A$ ,  $n$  and  $F$  represented, respectively, the electrode surface area, the number of electrons consumed in an electrochemical reaction and the Faraday constant.  $C_{Li^+}$  was the concentration of  $Li^+$  in an electrode material. For simplicity, except for  $\sigma$  value, other parameters appearing in equation (2) were assumed to be identical for all studied electrodes. Thus, the smaller  $\sigma$  value was, the larger  $D_{Li^+}$  value was obtained. As illustrated in figure d of Fig.5, electrode b had the minimum  $\sigma$  value among all studied electrodes. Consequently, the largest value of  $D_{Li^+}$  was delivered by electrode b. Therefore, anchoring petal-shaped micron-sized particles of CuBr onto the surface of the commercial Cu foil was a novel way to greatly enhance the  $D_{Li^+}$  value of the traditional graphite electrode.

To further explore the influence of the newly prepared foils on the electrochemical performance of the prepared graphite electrodes, the contact angles of the organic electrolyte of 1 M LiFP<sub>6</sub> against the newly prepared foils were measured and the results are shown in Fig.6. The contact angles for foil o, a, b and c were measured to be 42.7°, 30.3°, 17.1° and 28.8°, respectively. That is, the contact angle value of the copper foil was significantly decreased through immobilizing of micron-sized CuBr particles on its surface. Generally speaking, lower values of the contact angle would result in a higher adhesion between the liquid and the solid [32]. Thus, it was rational to think that the modification of micron-sized CuBr particles on the surface of the conventional copper foil greatly increased the adhesion between the organic electrolyte and the current collector, which would obviously reduce the interface resistance between the graphite powders and the current collector, being very favorable to the electrochemical property improvement of a conventional graphite electrode.

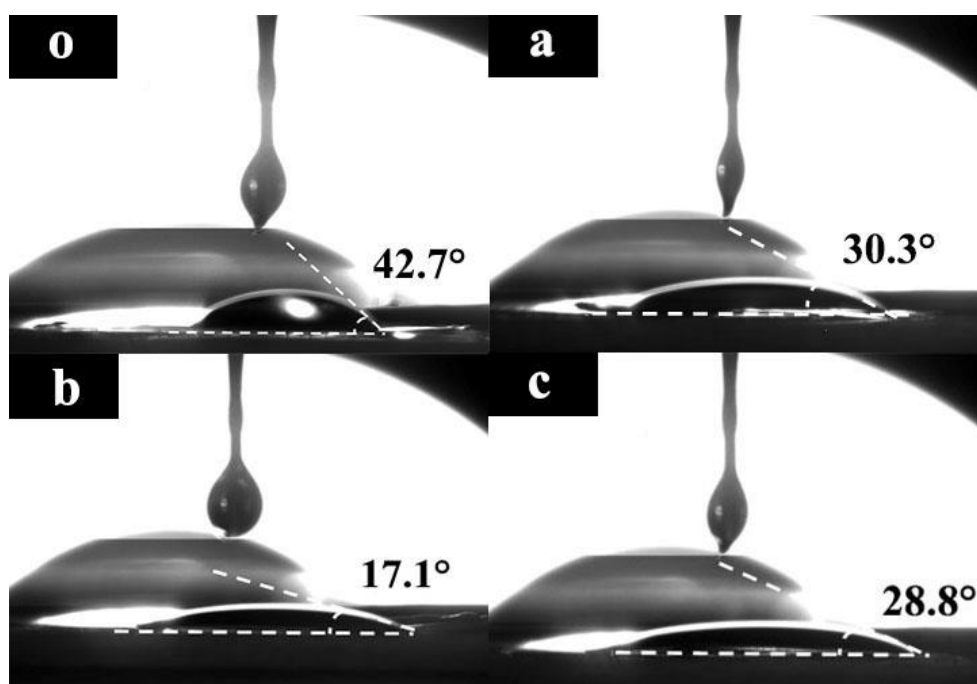


**Figure 6.** Photos obtained while measuring the contact angle of the studied foils. Photo o, a, b and c corresponded to the case of using foil o, a, b and c.

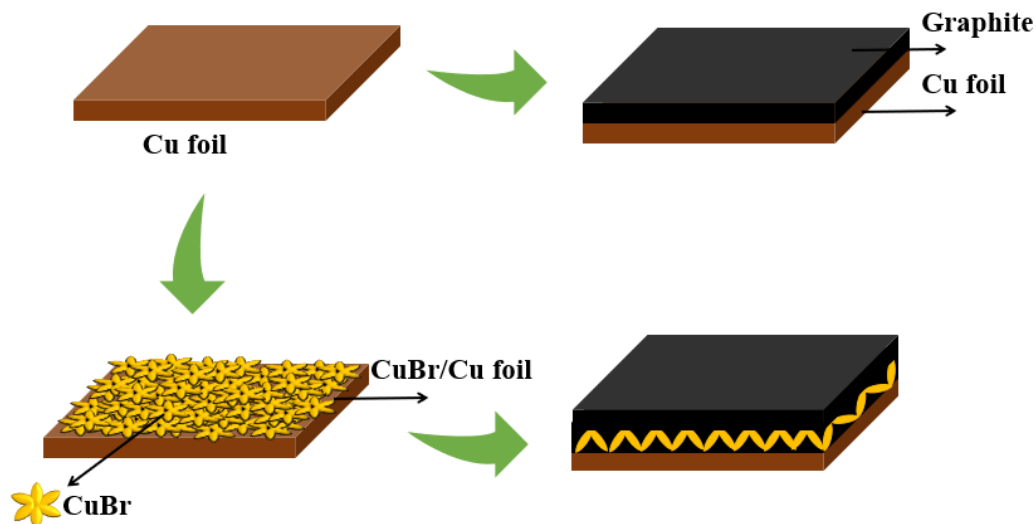


**Figure 7.** Diagrammatic sketches for preparing the conventional copper foil supported graphite electrode and foil b supported graphite electrode. The yellow flower shaped particles represented the petal-shaped micron-sized CuBr particles. The black and coppery part, respectively, corresponded to the graphite powder and the conventional copper foil.

To sum up, the following reasons were thought to be mainly responsible for the greatly enhanced electrochemical performances of the graphite electrode assembled using the newly prepared foils. (1) As shown in figure 1b, a rather uneven surface was created after the immobilization of the petal-shaped micron-sized CuBr particles on the surface of the conventional copper foil. To illustrate this, a diagrammatic sketch describing the connection between the graphite powders and the copper foil was shown in Fig.7. As shown by the upper part of Fig.7, for the conventional graphite electrode, graphite powders were directly pressed onto the surface of the conventional copper foil. While, in the case of using the newly prepared Cu foils, as shown by lower part of Fig.7, those petal-shaped micron-sized CuBr particles were intercalated into graphite powders, that is to say, the contacting area between the graphite particles and the current collector was significantly enlarged as compared to the case of using the conventional copper foil, which was very favorable to greatly abate the over-potential existing between the graphite particles and the current collector [29, 30]. (2) As indicated by CV curves in figure a of Fig.5, some novel substances have been activated to take part in the charge-discharge process of the graphite electrode when using the newly prepared foils, generating an increased DC value. (3) As displayed by figure c of Fig.5, a greatly reduced  $R_{ct}$  value was observed when employing foil a, b and c as the current collectors of the conventional graphite electrode, effectively indicating that using novel copper foils to replace the conventional Cu foil was a feasible approach to greatly cut down the values of the charge transfer resistance. (4) As discussed in the part concerning figure d of Fig.5, the  $D_{Li^+}$  value of the conventional graphite electrode was obviously enhanced through utilizing the newly prepared foils. (5) The wettability of the organic electrolyte on the current collector was remarkably ameliorated via employing the newly prepared foils. Summarily, an uneven surface morphology, some novel lithium storage substances, greatly reduced  $R_{ct}$  value,

obviously enhanced value of  $D_{Li^+}$  as well as the improved wettability were all analyzed to be the main reasons endowing electrode a, b and c, especially electrode b, an excellent electrochemical performance relative to that of the conventional graphite electrode.

#### 4. CONCLUSIONS

For the first time, petal-shaped micron-sized CuBr particles were immobilized onto the surface of the conventional copper foil via a very simple soaking method at room temperature in which the soaking solution only contained a copper foil, CuSO<sub>4</sub> and a surfactant of HTAB. In this work, the formation of CuBr was indicated by XPS spectra, and the surface morphologies of the prepared foils were observed by SEM. And then the resultant foils were employed as current collectors of the conventional graphite electrode, showing a facilitation effect on the electrochemical performance of the traditional graphite electrode. Specially, the DC value of the graphite electrode prepared using foil b at 1A g<sup>-1</sup> after 100 cycles (141 mAh g<sup>-1</sup>) was still about 3.9 times larger than that of the conventional graphite electrode (36 mAh g<sup>-1</sup>). As analyzed in this work, some novel lithium storage substances, the greatly reduced  $R_{ct}$  and the enhanced value of  $D_{Li^+}$  were thought to be the main reasons rendering the novel foils supported graphite electrodes delivering an improved electrochemical behavior as compared to the conventional graphite electrode. In a summary, a novel method for preparing petal-shaped micron-sized CuBr particles as well as a new way for promoting the electrochemical performance of the commercial graphite electrode was developed in this work, which was very beneficial to the development of micron-sized materials since no additional energy consumption was required, as well as, to the progress of graphite electrode based LIBs since no change of battery manufacturing process was needed, to our knowledge.

#### ACKNOWLEDGEMENTS

This work was funded by Science and Technology Project of Hebei Education Department (No. ZD2020327)

#### References

1. Y. Mao, W. Sun, X Yue, W. Hou, T. Deng, L. He, L. Fang, R. Sun, Z. Wang and K. Sun, *J. Power Sources*, 506 (2021) 230254.
2. R. Wang, Y. Yuan, J. Zhang, X. Zhong, J. Liu, Y. Xie, S. Zhong and Z. Xu, *J. Power Sources*, 501 (2021) 230006.
3. T. Greese and G. Reichenauer, *J. Power Sources*, 500 (2021) 229958.
4. S. Song, X. Qin, Y. Ruan, W. Li, Y. Xu, D. Zhang and J. Thokchom, *J. Power Sources*, 461 (2020) 228146.
5. P. Sehwat, A. Shabir, Abid, C.M. Julien and S. S. Islam, *J. Power Sources*, 501 (2021) 229709.
6. K. Brijesh, S. Vinayraj, P.C. Dhanush, K. Bindu and H.S. Nagaraja, *Electrochim. Acta*, 354 (2020) 136676.
7. B. Xing, H. Zeng, G. Huang, J. Jia, R. Yuan, C. Zhang, Q. Sun, Y. Cao, Z. Chen and B. Liu, *Electrochim. Acta*, 376 (2021) 138043.

8. W. Yuan, J. Luo, Z. Yan, Z. Tan and Y. Tang, *Electrochim. Acta*, 226 (2017) 89.
9. H. R. Kim and W. M. Choi, *Scripta Mater.*, 146 (2018) 100.
10. J. Chen, X. Wang, H. Gao, S. Yan, S. Chen, X. Liu and X. Hu, *Surf. Coat. Tech.*, 410 (2021) 126881.
11. L. Huang, F. Hu, Q. Ma and Y. Hu, *Tetrahedron Lett.*, 54 (2013) 3410.
12. L. Zheng, Y. Wang, X. Meng and Y. Chen, *Catal. Commun.*, 148 (2021) 106165.
13. M.V. Trigub, V.O. Troitskii and V.A. Dimaki, *Opt. Laser Technol.*, 139 (2021) 106929.
14. C. Gong, J. Chu, C. Yin, C. Yan, X. Hu, S. Qian, Y. Hu, K. Hu, J. Huang, H. Wang, Y. Wang, P. Wangyang, T. Lei, L. Dai, C. Wu, B. Chen, C. Li, M. Liao, T. Zhai and J. Xiong, *Adv. Mater.*, 31(2019) 1903580.
15. A.V. Mikheyenkov, V.E. Valiulin and A.F. Barabanov, *Physica B*, 599 (2020) 412533.
16. M. Yang, J.-J. Zhu and J.-J. Li, *J. Cryst. Growth*, 267 (2004) 283.
17. T. Subashini, B. Renganathan, A. Stephen and T. Prakash, *Mater. Sci. Semicond. Process.*, 88 (2018) 181.
18. H. Qin, C. Liu, N. Lv, W. He, J. Meng, Z. Fang and K. Guo, *Dyes Pigm.*, 174 (2020) 108071.
19. K. Ding, J. Han, X. Gao, L. Zhou and R. Qu, *Mater. Chem. Phys.*, 232 (2019) 354.
20. Y. Li, L. Yao, L.-Q. Zhang, A.-R. Liu, Y.-J. Zhang and S.-Q. Liu, *J. Electroanal. Chem.*, 730 (2014) 65.
21. X. Cai, J. Nie, C. Lu, F. Wang, C. Ma, G. Yang, Z. Chen and Y. Zhang, *Microporous Mesoporous Mater.*, 310 (2021) 110671.
22. M. Ganchev, R. Gergova, P. Terziyska, G. Popkirov and P. Vitanov, *Mater. Today: Proceedings*, 37 (2021) A16.
23. Y. Wu, G. Liu, D. Pan, H. Yuan and B. Li, *J. Hazard Mater.*, 413 (2021) 125394.
24. C. Zhang, Z. Wu, S. Jan, Z. Wang, S. Bennaceur, H.-K. Kim and X. Jin, *Electrochim. Acta.*, 390 (2021) 138800.
25. Z. Ma, Y. Zhuang, Y. Deng, X. Song, X. Zuo, X. Xiao and J. Nan, *J. Power Sources*, 376 (2018) 91.
26. K. Ding, H. Gu, C. Zheng, L. Liu, L. Liu, X. Yan and Z. Guo, *Electrochim. Acta.*, 146 (2014) 585.
27. C. Zhang, Z. Wu, S. Jan, Z. Wang, S. Bennaceur, H.-K. Kim and X. Jin, *Electrochim. Acta.*, 390 (2021) 138800.
28. K. Ding, J. Han, X. Gao, L. Zhou and R. Qu, *Mater. Chem. Phys.*, 232 (2019) 354.
29. K. Ding, J. Zhao, Y. Sun, Y. Chen, B. Wei, Y. Zhang and J. Pan, *Ceram. Int.*, 42 (2016) 19187.
30. K. Ding, B. Wei, Y. Zhang, C. Li, X. Shi and J. Pan, *Int. J. Electrochem. Sci.*, 12 (2017) 8381.
31. T.-F. Yi, H. Liu, Y.-R. Zhu, L.-J. Jiang, Y. Xie and R.-S. Zhu, *J. Power Sources*, 215(2012) 258.
32. K. Peta, T. Bartkowiak, P. Galek and M. Mendak, *Tribol. Int.*, 163 (2021) 107139.